Dynamic Friction Models for Road/Tire Longitudinal Interaction

Carlos Canudas-de-Wit*, Panagiotis Tsiotras†, Efstathios Velenis,†
Michel Basset‡ and Gerard Gissinger‡

SUMMARY

In this paper we derive a new dynamic friction force model for the longitudinal road/tire interaction for wheeled ground vehicles. The model is based on a dynamic friction model developed previously for contact-point friction problems, called the Lu-Gre model [7]. By assuming a contact patch between the tire and the ground we develop a partial differential equation for the distribution of the friction force along the patch. An ordinary differential equation (the lumped model) for the friction force is developed based on the patch boundary conditions and the normal force distribution along the contact patch. This lumped model is derived to closely approximate the distributed friction model. Contrary to common static friction/slip maps, it is shown that this new dynamic friction model is able to accurately capture the transient behaviour of the friction force observed during transitions between braking and acceleration. A velocity-dependent, steady-state expression of the friction force vs. the slip coefficient is also developed that allows easy tuning of the model parameters by comparison with steady-state experimental data. Experimental results validate the accuracy of the new tire friction model in predicting the friction force during transient vehicle motion. It is expected that this new model will be very helpful for tire friction modeling as well as for anti-lock braking (ABS) and traction control design.

*Corresponding author. Laboratoire d'Automatique de Grenoble, UMR CNRS 5528, ENSIEG-INPG, B.P. 46, 38 402 ST. Martin d'Hères, FRANCE, Tel: +33-4-76826380, Fax: +33-4-76826388, Email: canudas@lag.ensieg.inpg.fr

†School of Aerospace Engineering, Georgia Institute of Technology, Atlanta, GA 30332-0150, USA, Tel: (404) 894-9526, Fax: (404) 894-2760, Email: p.tsiotras@ae.gatech.edu, gte600q@prism.gatech.edu

‡Ecole Supérieure des Sciences Appliquées pour l'Ingénieur Mulhouse, 12, rue des Freres Lumiere, 68093 Mulhouse Cedex, FRANCE, Tel: +33-3-89336945, Fax: +33-3-89336949, Email: m.basset@essaim.univ-mulhouse.fr, g.gissinger@essaim.univ-mulhouse.fr

1 INTRODUCTION

The problem of predicting the friction force between the tire and the ground for wheeled vehicles is of enormous importance to automotive industry. Since friction is the major mechanism for generating forces on the vehicle, it is extremely important to have an accurate characterization of the magnitude (and direction) of the friction force generated at the ground/tire interface. However, accurate tire/ground friction models are difficult to obtain analytically. Subsequently, in the past several years, the problem of modeling and predicting tire friction has become an area of intense research in the automotive community. In particular, ABS and traction control systems rely on knowledge of the friction characteristics. Such systems have enhanced safety and maneuverability to such an extend, that they have become almost mandatory for all future passenger vehicles.

Traction control systems reduce or eliminate excessive slipping or sliding during vehicle acceleration and thus enhance the controllability and maneuverability of the vehicle. Proper traction control design has a paramount effect on safety and handling qualities for passenger vehicles. Traction control aims to achieve maximum torque transfer from the wheel axle to forward acceleration. Similarly, anti-lock braking systems (ABS) prohibit wheel lock and skidding during braking by regulating the pressure applied on the brakes, thus increasing lateral stability and steerability, especially during wet and icy road conditions. As with the case of traction control, the main difficulty in designing ABS systems is the nonlinearity and uncertainty of the tire/road models. In either case, the friction force at the tire/road interface is the main mechanism for converting wheel angular acceleration or deceleration (due to the motor torque or braking) to forward acceleration of deceleration (longitudinal force). Therefore, the study of the friction force characteristics at the road/tire interface is of paramount importance for the design of ABS and/or traction control systems. Moreover, tire friction models are also indispensable for accurately reproducing friction forces for simulation purposes. Active control mechanisms, such as ESP, TCS, ABS, steering control, active suspension, etc. may be tested and optimized using vehicle mechanical 3D simulators with suitable tire/road friction models.

A common assumption in most tire friction models is that the normalized tire friction μ

$$\mu = \frac{F}{F_n} = \frac{\text{Friction force}}{\text{Normal force}}$$

is a nonlinear function of the normalized relative velocity between the road and the tire (slip coefficient s) with a distinct maximum; see Fig. 1. In addition, it is understood that μ also depends on the velocity of the vehicle and road surface conditions, among other factors (see [6] and [15]). The curves shown in Fig. 1 illustrate how these factors influence the shape of μ.

The curves shown in Fig. 1 are derived empirically, based solely on steady-state (i.e., constant linear and angular velocity) experimental data [15, 3] in a highly controlled laboratory environment or using specially designed test vehicles. Under such steady-state conditions, experimental data seem to support

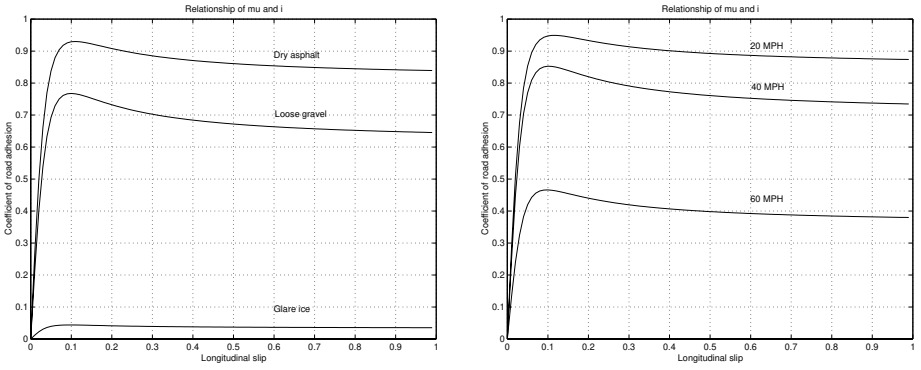

(a) (b)

Figure 1: Typical variations of the tire/road friction profiles for different road surface conditions (a), and different vehicle velocities (b). Curves given by Harned et al. [15].

the force vs. slip curves of Fig. 1. In reality, the linear and angular velocities can never be controlled independently and hence, such idealized steady-state conditions are not reached except during the rather uninteresting case of cruising with constant speed. The development of the friction force at the tire/road interface is very much a dynamic phenomenon. In other words, the friction force does not reach its steady-state value shown in Fig. 1 instantaneously, but rather exhibits transient behavior which may differ significantly from its steady-state value. Experiments performed in commercial vehicles, have shown that the tire/road forces do not necessarily vary along the curves shown Fig. 1, but rather "jump" from one value to another when these forces are displayed in the $\mu - s$ plane [25]. In addition, in realistic situations, these variations are most likely to exhibit hysteresis loops, clearly indicating the dynamic nature of friction.

In this paper, we develop a new, velocity-dependent, dynamic friction model that can be used to describe the tire/road interaction. The proposed model has the advantage that is developed starting from first principles based on a simple, point-contact dynamic friction model [7]. The parameters entering the model have a physical significance allowing the designer to tune the model parameters using experimental data. The proposed friction model is also velocity-dependent, a property that agrees with experimental observations. A simple parameter in the model can also be used to capture the road surface characteristics. Finally, in contrast to many other static models, our model is shown to be well-defined everywhere (even at zero rotational or linear vehicle velocities) and hence, is appropriate for any vehicle motion situations as well as for control law design. This is especially important during transient phases of the vehicle operation, such as during braking or acceleration.

2 STATIC SLIP/FORCE MODELS

In this paper we consider the simplified motion dynamics of a quarter-vehicle model. The system is then of the form

$$m\dot{v} = F \tag{1}$$
$$J\dot{\omega} = -rF + u\,, \tag{2}$$

where m is 1/4 of the vehicle mass and J, r are the inertia and radius of the wheel, respectively. v is the linear velocity of the vehicle, ω is the angular velocity of the wheel, u is the accelerating (or braking) torque, and F is the tire/road friction force. For the sake of simplicity, only longitudinal motion

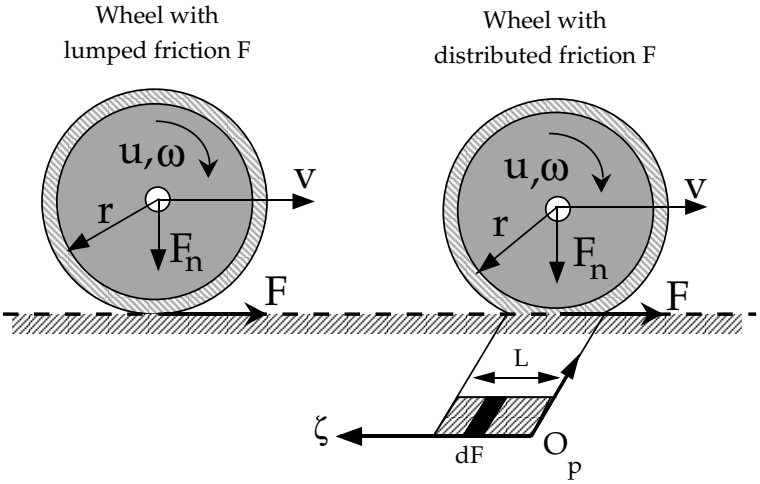

Figure 2: One-wheel system with lumped friction (left), and distributed friction (right).

will be considered in this paper. The lateral motion and well as combined longitudinal/lateral dynamics are left for future investigation. The dynamics of the braking and driving actuators, suspension dynamics, etc. are also neglected.

The most common tire friction models used in the literature are those of algebraic slip/force relationships. They are defined as one-to-one (memoryless) maps between the friction F, and the longitudinal slip rate s, which defined as

$$s = \begin{cases} s_b = \dfrac{r\omega}{v} - 1 & \text{if} \quad v > r\omega, \quad v \neq 0 \quad \text{for braking} \\ s_d = 1 - \dfrac{v}{r\omega} & \text{if} \quad v < r\omega, \quad \omega \neq 0 \quad \text{for driving} \end{cases} \tag{3}$$

The slip rate results from the reduction of the effective circumference of the tire as a consequence of the tread deformation due to the elasticity of the

tire rubber [19]. This, in turn, implies that the ground velocity v will not be equal to $r\omega$. The absolute value of the slip rate is defined in the interval $[0, 1]$. When $s = 0$ there is no sliding (pure rolling), whereas $|s| = 1$ indicates full sliding/skidding. It should be pointed out that in this paper we always define the relative velocity as $v_r = r\omega - v$. As a result, the slip coefficient in (3) is positive for driving and negative for braking. This is somewhat different than what is done normally in the literature, where the relative velocity (and hence the slip s) is kept always positive by redefining $v_r = v - r\omega$ in case of braking. Since we wish our results to hold for both driving and braking, we feel that it is more natural to keep the same definition for the relative velocity for both cases. This also avoids any inconsistencies and allows for easy comparison between the braking and driving regimes.

The slip/force models aim at describing the shapes shown in Fig. 1 via static maps $F(s) : s \mapsto F$. They may also depend on the vehicle velocity v, i.e. $F(s, v)$, and vary when the road characteristics change.

One of the most well-known models of this type is Pacejka's model (see, Pacejka and Sharp [21]), also known as the "Magic Formula." This model has been shown to suitably match experimental data, obtained under particular conditions of constant linear and angular velocity. The Pacejka model has the form[1]

$$F(s) = c_1 \sin(c_2 \arctan(c_3 s - c_4(c_3 s - \arctan(c_3 s)))) \,, \tag{4}$$

where the $c_i's$ are the parameters characterizing this model. These parameters can be identified by matching experimental data, as shown in Bakker et al. [3].

Another static model is the one proposed by Burckhardt [6]. The tire/road friction characteristic is of the form

$$F(s, v) = \left(c_1(1 - e^{-c_2 s}) - c_3 s\right) e^{-c_4 v} \,, \tag{5}$$

where $c_1, \cdots, c_4$ are some constants. This model has a velocity dependency, seeking to match variations like the ones shown in Fig. 1(b).

Kiencke and Daiss [16] neglect the velocity-dependent term in equation (5) and after approximating the exponential function in (5), they obtain the following expression for the friction/slip curve

$$F(s) = k_s \frac{s}{c_1 s^2 + c_2 s + 1} \,, \tag{6}$$

where k_s is the slope of the $F(s)$ vs. s curve at $s = 0$, and c_1 and c_2 are properly chosen parameters.

Alternatively, Burckhardt [5] proposes a simple, velocity-independent three-parameter model as follows

$$F(s) = c_1(1 - e^{-c_2 s}) - c_3 s \,. \tag{7}$$

[1] In the formulas that follow, it is assumed that $s \in [0, 1]$. Hence these formulas give the magnitude of the friction force. The sign of F is then determined from the sign of $v_r = r\omega - v$.

All the previous friction models are highly nonlinear in the unknown parameters, and thus they are not well-adapted to be used for on-line identification. For this reason, simplified models like

$$F(s) = c_1\sqrt{s} - c_2 s \tag{8}$$

have been proposed in the literature.

It is also well understood that the "constant" $c_i's$ in the above models, are not really invariant, but they may strongly depend on the tire characteristics (e.g., compound, tread type, tread depth, inflation pressure, temperature), on the road conditions (e.g., type of surface, texture, drainage, capacity, temperature, lubricant, etc.), and on the vehicle operational conditions (velocity, load); see, for instance the discussion in [20].

3 LUMPED DYNAMIC FRICTION MODELS

The static friction models of the previous section are appropriate when we have steady-state conditions for the linear and angular velocities. In fact, the experimental data used to validate the friction/slip curves are obtained using specialized equipment that allow independent linear and angular velocity modulation so as to transverse the whole slip range. This steady-state point of view is rarely true in reality, especially when the vehicle goes through continuous successive phases between acceleration and braking.

As an alternative to the static $F(s)$ maps, different forms of dynamic models can be adopted. The so-called "dynamic friction models" attempt to capture the transient behaviour of the tire-road contact forces under time-varying velocity conditions. Generally speaking, dynamic models can be formulated either as lumped or as distributed models, as shown in Fig. 2. A *lumped* friction model assumes a point tire-road friction contact. As a result, the mathematical model describing such a model is an ordinary differential equations that can be easily solved by time integration. *Distributed* friction models, on the other hand, assume the existence of a *contact patch* between the tire and the ground with an associated normal pressure distribution. This formulation results in a partial differential equation, that needs to be solved both in time and space.

A number of dynamic models have been proposed in the literature that can be classified under the term "dynamic friction models." One such model, for example, has been proposed by Bliman et al. in [4]. In that reference the friction is calculated by solving a differential equation of the following form

$$\begin{aligned} \dot{z} &= |v_r|Az + Bv_r \\ F(z, v_r) &= Cz + \operatorname{sgn}(v_r)D \end{aligned} \tag{9}$$

The matrix A is required to be Hurwitz of dimension either one or two, with the latter case being more accurate. Another lumped dynamic model that can be used to accurately predict the friction forces during transients is the LuGre

friction model [9]. The derivation of this model is discussed in great detail in Section 4. Before doing that, we next present two examples of frequently used dynamic friction models, the so-called "kinematic model" and the "Dahl model". This will allow us to motivate our introduction in Section 4 of a new distributed (and later in Section 5 of an average lumped) friction model. In addition, it will be shown that these two commonly used lumped models are not able to reproduce the steady-state characteristics, similar to those of Pacejka's "Magic Formula."

3.1 Kinematic-Based Models

These models are derived from the idealization of a contact point deformation and from kinematic considerations (velocity relations between the points that concern the tire deformations). Their derivation follows semi-empirical considerations and assumes that the contact forces result from the product of the tire deformation and the tire stiffness.

An example of a two-dimensional model characterizing the lateral force and the aligning moment, can be found in [18]. A brush model for the longitudinal tire dynamics has been derived in [10, 2].

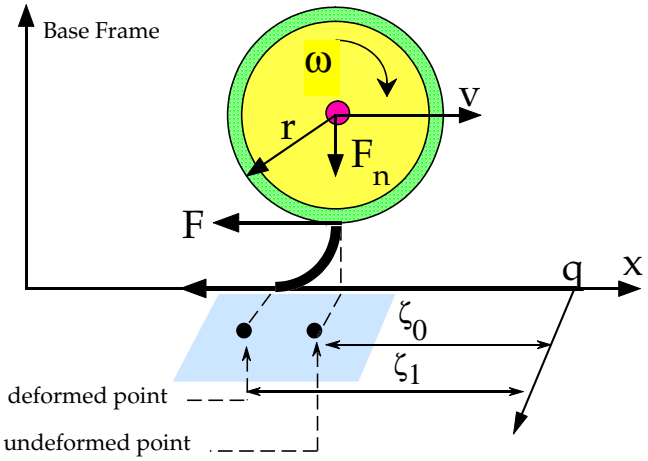

Figure 3: View of the contact area with the position of the undeformed contact point ζ_0, and the point ζ_1 that deforms under longitudinal shear forces during a brake phase.

For simplicity, next we only discuss the braking case. The traction case follows a similar development, with an appropriate definition of z. In that case, the relaxation length may be defined as the wheel arc length required to build friction.

A model for the longitudinal dynamics in [10] is derived by defining the *normalized* longitudinal slip z as

$$z = \frac{\zeta_1 - \zeta_0}{\zeta_0} \tag{10}$$

where ζ_1 locates a hypothetical element which follows the road, and it defines the distance from the *deformed* wheel point to a forward point q. ζ_0 locates a hypothetical element which in undeformed under longitudinal shear forces, and defines the distance from the *undeformed* wheel point (i.e. center of the wheel's rotational axis) to a forward point q as shown in Fig. 3. The undeformed point ζ_0 and the forward point q are moving at the same ground speed v, thus the distance ζ_0 is constant with respect to the moving point q. The length ζ_0 is known as the longitudinal relaxation length.

Differentiating z in (10) with respect to time, and noticing that $\dot{\zeta}_0 = |v|$, $\dot{\zeta}_1 = \text{sgn}(v) r\omega$, we get[2]

$$\frac{1}{\sigma}\frac{dz}{dt} = v_r \text{sgn}(v) - |v| z \tag{11}$$

$$F = h(z) \tag{12}$$

where v is the linear velocity, $v_r = r\omega - v$ is the relative velocity, and the friction force F is defined by the function $h(z)$ that describes the stationary slip characteristics. In the simplest case, $h(z)$ is given by a linear relationship between the longitudinal slip and the tire (linear) stiffness k,

$$h(z) = kz$$

The constant $1/\sigma = \zeta_0$ is called the relaxation length, and can be defined as the distance required to reach the steady-state value of F

$$F_{ss} = h(z_{ss}) = kz_{ss} = k\frac{r\omega - v}{v} = ks$$

after a step change of the slip longitudinal velocity, $s = s_b = v_r/v = (r\omega - v)/v$. The role of the relaxation length $1/\sigma$ in equation (11), can be better understood by rewriting this equation in terms of the spatial coordinate η,

$$\eta(t) = \int_0^t |v(\tau)| d\tau$$

rather than as a time-differential equation, i.e.,

$$\frac{1}{\sigma}\frac{dz}{dt} = \frac{1}{\sigma}\frac{dz}{d\eta}\frac{d\eta}{dt} = v_r \text{sgn}(v) - |v| z \tag{13}$$

$$\frac{1}{\sigma}\frac{dz}{d\eta} = -z + \frac{v_r}{v} = -z + s \tag{14}$$

Equation (14) can thus be seen as a first order spatial equation with the sliding velocity s as its input. It thus becomes clear that σ represents the *spatial* constant of this equation.

As pointed out in [10], this model works well for high speeds, but it generates lightly damped oscillations at low speeds. The reason for this is that at quasi-steady-state regimes, z is close to its steady-state value ($z \approx s$) , and the friction

[2] In this expression both positive and negative v are considered.

F is dominated by its spring-like behaviour ($F \approx kz$), resulting in a lightly damped mechanical system. Additional considerations are necessary to make this model consistent for all possible changes in the velocity sign. This restricts the usefulness of this model for tire friction analysis and control development. Reference [10] actually provides a twelve-step algorithm for implementing this model in simulations.

3.2 The Dahl Model

The Dahl model [11] was developed for simulating control systems with friction. The starting point of Dahl's model is the stress-strain curve in classical solid mechanics [22] and [23]; see Fig. 4. When subject to stress, the friction force

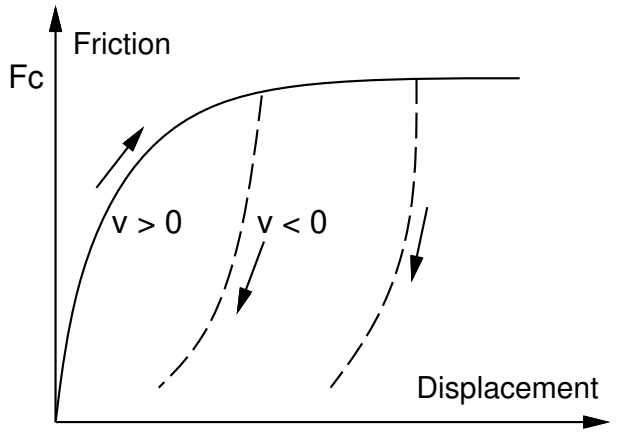

Figure 4: Friction force as a function of displacement for the Dahl's model.

increases gradually until rupture occurs. Dahl modeled the stress-strain curve by a differential equation. Let x_r be the relative displacement, $v_r = dx_r/dt$ be the relative velocity, F the friction force, and F_c the maximal friction force (Coulomb force). Dahl's model then takes the form,

$$\frac{dF}{dx_r} = \sigma_0 \left(1 - \frac{F}{F_c}\text{sgn}(v_r)\right)^{\beta} \tag{15}$$

where σ_0 is the stiffness coefficient and β is a parameter that determines the shape of the stress-strain curve. The value $\beta = 1$ is most commonly used. Higher values will give a stress-strain curve with a sharper bend. The friction force $|F|$ will never be larger than F_c if its initial value is such that $|F(0)| < F_c$. When integrating (15) for step changes of v_r, a monotonic growing of $F(t)$ can be observed. Therefore, Dahl's model cannot exhibit a maximum peak, as suggested by Pacejka's "Magic Formula."

It is also important to remark that in this model the friction force is only a function of the displacement and the sign of the relative velocity. This implies

that the evolution of the friction force in the $F - x_r$ plane will only depend on the sign of the velocity, but not on the magnitude of v_r. This implies rate-independent hysteresis loops in the $F - x_r$ plane [4].

To obtain a time-domain model, Dahl observed that,

$$\frac{dF}{dt} = \frac{dF}{dx_r}\frac{dx_r}{dt} = \frac{dF}{dx_r}v_r = \sigma_0 \left(1 - \frac{F}{F_c}\text{sgn}(v_r)\right)^{\beta} v_r \tag{16}$$

For the case $\beta = 1$, the model (16) can be written as

$$\frac{dF}{dt} = \sigma_0(v_r - \frac{F}{F_c}|v_r|) \tag{17}$$

or in its state model description,

$$\begin{aligned} \frac{dz}{dt} &= v_r - \sigma_0 \frac{z}{F_c}|v_r| && (18)\\ F &= \sigma_0 z && (19) \end{aligned}$$

with z being the relative displacement. Note the difference in the interpretation of z between the kinematic and Dahl models. In the Dahl model z represents the actual relative displacement, where in the kinematic model it represents the *normalized* relative displacement. Moreover, whereas in (18) the coefficient of z depends on the relative velocity v_r, in the kinematic model (11) it depends on the vehicle velocity v.

Introducing the *relative* length distance η_r as,

$$\eta_r(t) = \int_0^t |v_r(\tau)|d\tau,$$

the Dahl model becomes

$$\frac{1}{\sigma_0}\frac{dF}{d\eta_r} = -\frac{1}{F_c}F + \text{sgn}(s) \tag{20}$$

where we have used the fact that $\text{sgn}(v_r) = \text{sgn}(s)$. In this coordinate, the Dahl model behaves as a linear, space-invariant system with the sign of the longitudinal slip velocity as its input. The motion in the $F - \eta_r$ plane is thus independent of the magnitude of the slip velocity.

3.3 Comparison Between Kinematic and Dahl Models

It is also instructive to compare the kinematic model and the Dahl model. First, note that the steady-state values for each model are,

$$F_{ss}^{\text{kin}} = ks, \qquad F_{ss}^{\text{Dahl}} = F_c\text{sgn}(s)$$

Since $|s| \leq 1$, then k and F_c represent the maximum values that friction can take. In steady state, the kinematic model predicts a linear behaviour with

respect to s, whereas the Dahl model predicts a discontinuous form with values in the set $[-F_c, F_c]$.

In the neighborhood of $v_r = 0$, both models predict similar linearized presliding (spring-like) behaviour,

$$F_{ss}^{\text{kin}} \approx k\sigma\eta_r, \qquad F_{ss}^{\text{Dahl}} \approx \sigma_0\eta_r \tag{21}$$

Nonetheless, there are some differences when comparing the complete dynamic equations of both models. To this end, consider the particular form $h(z) = kz$ in equation (12). Then the spatial representations of both models in the η, and the η_r coordinates are given as,

$$\frac{1}{\sigma_0}\frac{dF^{\text{Dahl}}}{d\eta_r} = -\frac{1}{F_c}F^{\text{Dahl}} + \text{sgn}(s) \tag{22}$$

$$\frac{1}{k\sigma}\frac{dF^{\text{kin}}}{d\eta} = -\frac{1}{k}F^{\text{kin}} + \text{sgn}(s) \tag{23}$$

Let $F_c = k$, and $\sigma_0 = k\sigma$, then both models looks similar. Note however that they are defined in different coordinates. This changes the interpretation that may be given to the relaxation length constant: $F_c\sigma_0$ describes the relaxation length of the Dahl model with respect to the *relative* (sliding) distance, whereas $1/\sigma$ represents the relaxation length of the kinematic model defined with respect to the *absolute* (total) traveled longitudinal distance.

Note also that both of these models do not exhibit a maximum for values $|s| < 1$, as suggested by experimental data and also by Pacejka's formula. However, the kinematic model can be modified by redefining the function $h(z)$ in (12) so as to produce a steady-state behaviour similar to the one predicted by the "Magic Formula" [2].

3.4 The Lumped LuGre Model

The LuGre model is an extension of the Dahl model that includes the Stribeck effect (see, [7]). This model will be used as a basis for further developments for the final model proposed in this paper. The lumped, LuGre model as proposed in [9], and [8] is given as,

$$\dot{z} = v_r - \frac{\sigma_0|v_r|}{g(v_r)}z \tag{24}$$

$$F = (\sigma_0 z + \sigma_1\dot{z} + \sigma_2 v_r)\, F_n \tag{25}$$

with

$$g(v_r) = \mu_c + (\mu_s - \mu_c)e^{-|v_r/v_s|^\alpha} \tag{26}$$

where σ_0 is the rubber longitudinal lumped stiffness, σ_1 the rubber longitudinal lumped damping, σ_2 the viscous relative damping, μ_c the normalized Coulomb friction, μ_s the normalized static friction, $(\mu_c \leq \mu_s)$, v_s the Stribeck relative velocity, F_n the normal force, $v_r = r\omega - v$ the relative velocity, and z the internal

friction state. The constant parameter α is used to capture the steady-steady friction/slip characteristic[3].

In contrast to the Dahl model, the lumped LuGre model does exhibit a maximum friction for $|s| \leq [0, 1]$, but it still displays a discontinuous steady-state characteristic, at zero relative velocity. Nevertheless, by letting the internal bristle deflection z depend on both the time and the contact position ζ along the contact patch, it is possible to show that this model will have the appropriate steady-state properties. This is discussed next.

4 THE LUGRE DISTRIBUTED MODEL

Distributed models assume the existence of an area of contact (or patch) between the tire and the road, as shown in Fig. 2. This patch represents the projection of the part of the tire that is in contact with the road. With the contact patch is associated a frame O_p, with ζ-axis along the length of the patch in the direction of the tire rotation. The patch length is L.

4.1 Brief Review of Existing Models

Distributed dynamical models, have been studied previously, for example, in the works of Bliman et al. [4]. In these models, the contact patch area is discretized to a series of elements, and the microscopic deformation effects are studied in detail. In particular, Bliman at al. [4] characterize the elastic and Coulomb friction forces at each point of the contact patch, and they give the aggregate effect of these distributed forces by integrating over the whole patch area. They propose a second order rate-independent model (similar to Dahl's model), by applying the point friction model (9) to a rubber element situated at ζ at time t. By letting $z(\zeta, t)$ denote the corresponding friction state, they obtain the partial differential equation

$$\frac{\partial z}{\partial t} + r\omega \frac{\partial z}{\partial \zeta} = |v_r| A z + B v_r, \qquad z(\zeta, 0) = z(0, t) = 0 \tag{27}$$

$$F(t) = \frac{F_n}{L} \int_0^L C z(\zeta, t)\, d\zeta \tag{28}$$

They also show that, under constant v and ω, there exists a choice of parameters A, B and C that closely match a curve similar to the one characterizing the "Magic Formula."

In [25] van Zanten et al. use a distributed brush model. The contact patch is described by a brush-type model where the displacement of each bristle is

[3]The model in (25) differs from the point-contact LuGre model in [7] in the way that the function $g(v)$ is defined. Here we propose to use $\alpha = 1/2$ instead of $\alpha = 2$ as in the LuGre point-contact model in order to better match the pseudo-stationary characteristic of this model (map $s \mapsto F(s)$) with the shape of the Pacejka's model.

characterized by the state z_i, $i = 1, \ldots, N$. The discretized version of this model, in its simplest form, is given by

$$\frac{dz_i}{dt} = v - \omega r - \frac{z_i - z_{i-1}}{L/N}\,\omega r \tag{29}$$

$$F = \sum_{i=1}^{N} c_i z_i \tag{30}$$

where N is the number of discrete elements (bristles) and c_i is the stiffness of the bristle. The imposed boundary condition $dz_1/dt = 0$ implies that the bristle at the beginning of the contact area has no displacement.

4.2 Distributed LuGre Model

One can also extend the point friction model (24)-(25) to a distributed friction model along the patch by letting $z(\zeta, t)$ denote the friction state (deflection) of the bristle/patch element located at the point ζ along the patch at a certain time t. At every time instant $z(\zeta, t)$ provides the deflection distribution along the contact patch. The model (24)-(25) can now be written as

$$\frac{d\,z}{dt}(\zeta, t) = v_r - \frac{\sigma_0 |v_r|}{g(v_r)}\,z \tag{31}$$

$$F = \int_0^L dF(\zeta, t)\,, \tag{32}$$

with $g(v_r)$ defined as in (26) and where

$$dF(\zeta, t) = \left(\sigma_0\, z(\zeta, t) + \sigma_1\, \frac{\partial z}{\partial t}(\zeta, t) + \sigma_2 v_r\right) dF_n(\zeta, t)\,,$$

where $dF(\zeta, t)$ is the differential friction force developed in the element $d\zeta$ and $dF_n(\zeta, t)$ is the differential normal force applied in the element $d\zeta$ at time t. This model assumes that the contact velocity of each differential state element is equal to v_r.

Assuming a steady-state normal force distribution $dF_n(\zeta, t) = dF_n(\zeta)$ and introducing a normal force density function $f_n(\zeta)$ (force per unit length) along the patch, i.e.,

$$dF_n(\zeta) = f_n(\zeta) d\zeta$$

one obtains the total friction force as

$$F(t) = \int_0^L (\sigma_0 z(\zeta, t) + \sigma_1 \frac{\partial z}{\partial t}(\zeta, t) + \sigma_2 v_r) f_n(\zeta) d\zeta \tag{33}$$

Noting that[4] $\dot{\zeta} = |r\omega|$, and that

$$\frac{d\,z}{dt}(\zeta, t) = \frac{\partial z}{\partial \zeta}\frac{\partial \zeta}{\partial t} + \frac{\partial z}{\partial t},$$

[4]It is assumed here that the origin of the ζ-frame changes location when the wheel velocity reverses direction, such that $\dot{\zeta} = r\omega$, for $\omega > 0$, and $\dot{\zeta} = -r\omega$, for $\omega < 0$.

we have that equation (31) describes a partial differential equation, i.e.

$$\frac{\partial z}{\partial \zeta}(\zeta,t)\,|r\omega| + \frac{\partial z}{\partial t}(\zeta,t) = v_r - \frac{\sigma_0|v_r|}{g(v_r)}\,z(\zeta,t) \tag{34}$$

that should be solved in both in time and space. More details on the derivation of this distributed friction model are given in Appendix A.

4.3 Steady-State Characteristics

The time steady-state characteristics of the model (31)-(32) are obtained by setting $\frac{\partial z}{\partial \zeta}(\zeta,t) \equiv 0$ and by imposing that the velocities v and ω are constant. Enforcing these conditions in (34) results in

$$\frac{\partial z(\zeta,t)}{\partial \zeta} = \frac{1}{|\omega r|}\left(v_r - \frac{\sigma_0|v_r|}{g(v_r)}z(\zeta,t)\right) \tag{35}$$

At steady-state, v, ω (and hence v_r) are constant, and (35) can be integrated along the patch with the boundary condition $z(0,t) = 0$. A simple calculation shows that

$$z_{ss}(\zeta) \;\; = \;\; \mathrm{sgn}(v_r)\frac{g(v_r)}{\sigma_0}\left(1 - e^{-\frac{\sigma_0}{g(v_r)}\,|\frac{v_r}{\omega r}|\zeta}\right) = c_2(1 - e^{c_1\zeta}) \tag{36}$$

where

$$c_1 = -\frac{\sigma_0}{g(v_r)}\,\left|\frac{v_r}{\omega r}\right|, \qquad c_2 = \mathrm{sgn}(v_r)\frac{g(v_r)}{\sigma_0} \tag{37}$$

Notice that when $\omega = 0$ (locked wheel case) the distributed model, and hence the steady-state expression (36) collapses into the one predicted by the standard point-contact LuGre model. This agrees with the expectation that for a locked wheel the friction force is only due to pure sliding.

The steady-state value of the total friction force is calculated from (33)

$$F_{ss} = \int_0^L (\sigma_0 z_{ss}(\zeta) + \sigma_2 v_r) f_n(\zeta) d\zeta \tag{38}$$

To proceed with the calculation of F_{ss} we need to postulate a distribution for the normal force $f_n(\zeta)$. The typical form of the normal force distribution reported in the literature [24, 19, 14, 13], is shown in Fig. 5. However, for the sake of simplicity, other forms can be adopted. Some examples are given next.

- *Constant norm distribution.* A simple result can be derived if we assume uniform load distribution, as done in [9] and [12]. For uniform normal load

$$f_n(\zeta) = \frac{F_n}{L}, \quad 0 \le \zeta \le L \tag{39}$$

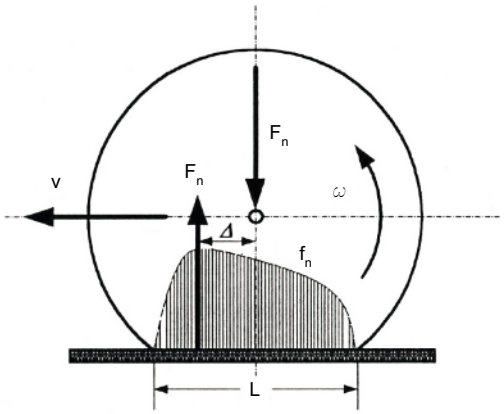

Figure 5: Typical normal load distribution along the patch; taken from [14].

and one obtains,

$$F_{ss} = \left(\text{sgn}(v_r) g(v_r) \Big[1 - \frac{Z}{L}(1 - e^{-L/Z}) \Big] + \sigma_2 v_r \right) F_n \tag{40}$$

where

$$Z = \left| \frac{\omega r}{v_r} \right| \frac{g(v_r)}{\sigma_0} \tag{41}$$

- *Exponentially decreasing distribution.* In this case, the decrease of the normal load along the patch shown in Fig. 5 is approximated with an exponentially decreasing function

$$f_n(\zeta) = e^{-\lambda(\frac{\zeta}{L})} f_{n0}, \qquad 0 \le \lambda, \quad 0 \le \zeta \le L \tag{42}$$

where $f_n(0) = f_{n0}$ denotes the distributed normal load at $\zeta = 0$. This particular choice will become clear later on, when we reduce the infinite dimension distributed model to a simple lumped one having only one state variable. Moreover, for $\lambda > 0$ we have a strictly decreasing function of f_n. With the choice (42) one obtains

$$F_{ss} = \sigma_0 c_2 k_1 \Big(1 - e^{-\lambda} + k_2 e^{(-\lambda + CL)} + k_2 \Big) + \sigma_2 v_r k_1 (1 - e^{-\lambda}) \tag{43}$$

where

$$k_1 = \frac{f_{n0} L}{\lambda} \qquad \text{and} \qquad k_2 = \frac{\lambda}{c_1 L - \lambda}$$

The details of these calculations are given in Appendix B. The value of f_{n0} can be computed from λ, L and the total normal load F_n acting on

the wheel shaft. That is,

$$\begin{aligned} F_n &= \int_0^L f_n(\zeta)\, d\zeta = f_{n0} \int_0^L e^{-\frac{\lambda}{L}\zeta}\, d\zeta \\ &= -\frac{L}{\lambda} f_{n0} \Big[e^{-\frac{\lambda}{L}\zeta} \Big]_0^L = -\frac{L}{\lambda} f_{n0} \left(e^{-\lambda} - 1 \right) \\ &= \frac{L}{\lambda} f_{n0} \left(1 - e^{-\lambda} \right) \end{aligned} \tag{44}$$

which yields,

$$f_{n0} = F_n \frac{\lambda}{(1 - e^{-\lambda})L} \tag{45}$$

- *Distributions with zero boundary conditions.* As shown in Fig. 5, a realistic force distribution has, by continuity, zero values for the normal load at the boundaries of the patch. Several forms satisfy this constraint. Some possible examples proposed herein are given below:

$$f_n(\zeta) = \frac{3F_n}{2L} \left[1 - \left(\frac{\zeta - L/2}{L/2} \right)^2 \right] \qquad \text{parabolic} \tag{46}$$

or,

$$f_n(\zeta) = \frac{\pi F_n}{2L} \sin(\pi\zeta/L) \qquad \text{sinusoidal} \tag{47}$$

or,

$$f_n(\zeta) = \frac{\gamma^2 L^2 + \pi^2}{\pi L(e^{-\gamma L} + 1)} \exp^{-\gamma\zeta} \sin(\pi\zeta/L) \qquad \text{sinusoidal/exponential} \tag{48}$$

where F_n denotes the total normal load.

4.4 Relation with the Magic Formula

The previously derived steady-state expressions, depend on both v and ω. They can also be expressed as a function of s and either v or ω. For example, for the constant distribution case, we have that $F_{ss}(s)$, can be rewritten as:

- *Driving case.* In this case $v < r\omega$, see also (3), and the force at steady-state is given by

$$F_d(s) = \operatorname{sgn}(v_r) F_n g(s) \left(1 + \frac{g(s)}{\sigma_0 L|s|} (e^{-\frac{\sigma_0 L|s|}{g(s)}} - 1) \right) + F_n \sigma_2 r\omega s \tag{49}$$

with $g(s) = \mu_c + (\mu_s - \mu_c)\, e^{-|r\omega s/v_s|^\alpha}$, for some constant ω, and $s = s_d$.

- *Braking case.* Noticing that the following relations hold between the braking s_b and the driving s_d slip definitions,

$$r\omega s_d = v s_b, \qquad s_d = \frac{s_b}{s_b + 1}$$

the steady-state friction force for the braking case can be written as

$$F_b(s) = \operatorname{sgn}(v_r) F_n g(s) \left(1 + \frac{g(s)|1+s|}{\sigma_0 L |s|} (e^{-\frac{\sigma_0 L |s|}{g(s)|1+s|}} - 1) \right) + F_n \sigma_2 v s \tag{50}$$

where $g(s) = \mu_c + (\mu_s - \mu_c)\, e^{-|vs/v_s|^\alpha}$, for constant v, and $s = s_b$; see also (3).

Remark: Note that the above expressions depend not only on the slip s, but also on either the vehicle velocity v or the wheel velocity ω, depending on the case considered (driving or braking). Therefore static plots of F vs. s can only be obtained for a specified (constant) velocity. This dependence of the steady-state force/slip curves on vehicle velocity is evident in experimental data found in the literature. Nonetheless, it should be stressed here that it is impossible to reproduce such a curves form experimental data obtained from standard vehicles during normal driving conditions, since v and ω cannot be independently controlled. For that, specially design equipment is needed. Figure 6(a) shows the steady-state dependence on the vehicle velocity for the braking case, using the data given in Table 1.

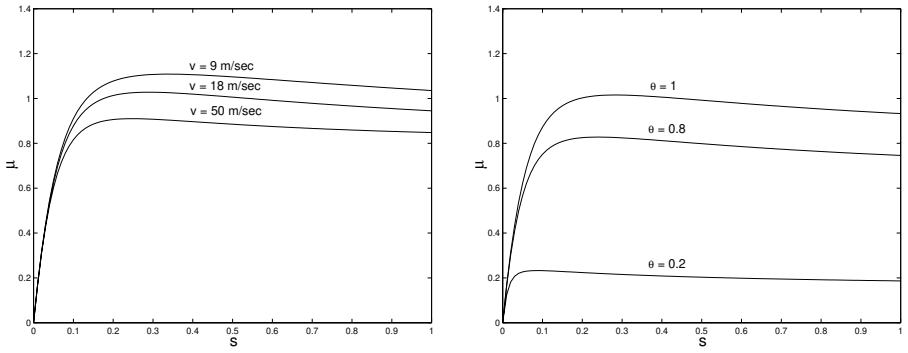

(a) (b)

Figure 6: Static view of the distributed LuGre model with uniform force distribution (braking case) under: (a) different values for v, (b) different values for θ with $v = 20\,\mathrm{m/s} = 72\,\mathrm{Km/h}$. These curves show the normalized friction $\mu = F(s)/F_n$, as a function of the slip velocity s.

Table 1: Data used for the plots in Fig. 6

Parameter	Value	Units
σ_0	181.54	[1/m]
σ_2	0.0018	[s/m]
μ_c	0.8	[-]
μ_s	1.55	[-]
v_s	6.57	[m/s]
L	0.2	[m]

4.5 Dependency on Road Conditions

The level of tire/road adhesion, can be modeled by introducing a multiplicative parameter θ in the function $g(v_r)$. To this aim, we substitute $g(v_r)$ by

$$\tilde{g}(v_r) = \theta g(v_r)\,,$$

where $g(v_r)$ is the nominal known function given in (26). Computation of the function $F(s,\theta)$, from equation (50) as a function of θ, gives the curves shown in Fig. 6(b). These curves match reasonably well the experimental data shown in Fig. 1(a), for several coefficients of road adhesion using the parameters shown in Table 1. Hence, the parameter θ, can suitably describe the changes in the road characteristics.

We also note that the steady-state representation of equations (49) or (50) can be used to identify most of the model parameters by fitting this model to experimental data. These parameters can also be used in a simple one-dimensional lumped model, which can be shown to suitably approximate the (average) solution of the partial differential equation (31) and (32). This approximation is discussed next.

5 AVERAGE LUMPED MODEL

It is clear that the distributed model captures reality better than the lumped, point contact model. It is also clear that in order to use the distributed model for control purposes it is necessary to choose a discrete number of states to describe the dynamics for each tire. This has the disadvantage that a possibly large number of states is required to describe the friction generated at each tire. Alternatively, one could define a *mean friction state* $\bar{z}$ for each tire and then derive an *ordinary differential equation* for $\bar{z}$. This will simplify the analysis and can also lead to much simpler control design synthesis procedures for tire friction problems.

To this end, let us define

$$\bar{z}(t) \quad \equiv \quad \frac{1}{F_n}\int_0^L z(\zeta,t) f_n(\zeta) d\zeta \tag{51}$$

where F_n is the total normal force, given by

$$F_n = \int_0^L f_n(\zeta)\, d\zeta$$

Thus,

$$\dot{\bar{z}}(t) = \frac{1}{F_n} \int_0^L \frac{\partial z}{\partial t}(\zeta, t) f_n(\zeta) d\zeta \tag{52}$$

Using (34) we get

$$\begin{aligned}
\dot{\bar{z}}(t) &= \frac{1}{F_n} \int_0^L \Big(v_r - \frac{\sigma_0 |v_r|}{g(v_r)} z(\zeta, t) - \frac{\partial z(\zeta, t)}{\partial \zeta} |\omega r| \Big) f_n(\zeta) d\zeta \\
&= v_r - \frac{\sigma_0 |v_r|}{g(v_r)} \bar{z}(t) - \frac{|\omega r|}{F_n} \int_0^L \frac{\partial z(\zeta, t)}{\partial \zeta} f_n(\zeta) d\zeta \\
&= v_r - \frac{\sigma_0 |v_r|}{g(v_r)} \bar{z}(t) - \frac{|\omega r|}{F_n} \Big[z(\zeta, t) f_n(\zeta) \Big]_0^L + \frac{|\omega r|}{F_n} \int_0^L z(\zeta, t) \frac{\partial f_n(\zeta)}{\partial \zeta} d\zeta
\end{aligned}$$

The term in the square brackets describes the influence of the boundary conditions, whereas the integral term accounts for the particular form of the force distribution.

From (33) the friction force is

$$\begin{aligned}
F(t) &= \int_0^L \left(\sigma_0\, z(\zeta, t) + \sigma_1 \frac{\partial z}{\partial t}(\zeta, t) + \sigma_2 v_r \right) f_n(\zeta)\ d\zeta \\
&= (\sigma_0 \bar{z}(t) + \sigma_1 \dot{\bar{z}}(t) + \sigma_2 v_r)\ F_n
\end{aligned}$$

As a general goal, one wishes to introduce normal force distributions, that leads to the following form for the lumped LuGre model,

$$\dot{\bar{z}}(t) = v_r - \frac{\sigma_0 |v_r|}{g(v_r)} \bar{z}(t) - \kappa(t) |\omega r| \bar{z}(t) \tag{53}$$

$$F(t) = (\sigma_0 \bar{z}(t) + \sigma_1 \dot{\bar{z}}(t) + \sigma_2 v_r)\, F_n \tag{54}$$

where $\kappa(t)$ is defined as:

$$\kappa(t) = \frac{1}{F_n\, \bar{z}} \left\{ \Big[z(\zeta, t) f_n(\zeta) \Big]_0^L - \int_0^L z(\zeta, t) \frac{\partial f_n(\zeta)}{\partial \zeta} d\zeta \right\} \tag{55}$$

and F_n as above. When comparing this model with the point contact LuGre model (24)-(25), it is clear that κ captures the distributed nature of the former model. It is also expected that $\kappa > 0$, so that the map $v_r(t) \mapsto F(t)$ preserves the passivity properties of the point contact LuGre model [7, 1].

For the case of normal load distributions with zero boundary conditions we have $f_n(0) = f_n(L) = 0$ and equation (55) yields

$$\kappa(t) = - \frac{\int_0^L z(\zeta, t) f_n'(\zeta) d\zeta}{\int_0^L z(\zeta, t) f_n(\zeta) d\zeta} \tag{56}$$

where $f_n'(\zeta) = \partial f_n(\zeta) / \partial \zeta$.

5.1 Influence of the Force Distribution on $\kappa(t)$

Depending on the postulated normal force distribution density function, several expressions for the average lumped model can be developed. For instance, κ may be a constant, an explicit or an implicit function of the mean friction state $\bar{z}$. We study some of these forms next.

Parabolic Distribution

For a parabolic normal force distribution $f_n(\zeta)$ is given by (46). In order to compute κ from (56) we now make the assumption that $z(\zeta,t)$ is a separable function of ζ and t, namely, $z(\zeta,t) = \varphi(\zeta)\theta(t)$ for some (time-independent) deflection function $\varphi(\zeta)$, $0 \le \zeta \le L$ and some (space-independent) time function $\theta(t)$, $t \ge 0$. From the discussion in Section 4.2 $\varphi(\zeta)$ can be interpreted as the deflection of the bristle along the patch at position ζ. We impose the boundary condition that $\varphi(0) = 0$, since there is no deflection for the first bristle element. Under the reasonable assumption that the deflection of the bristles builds gradually along the patch, we postulate that $\varphi(\zeta) = \zeta$ and hence

$$\begin{aligned} \kappa &= -\frac{\int_0^L \varphi(\zeta)\theta(t) f_n'(\zeta) d\zeta}{\int_0^L \varphi(\zeta)\theta(t) f_n(\zeta) d\zeta} = -\frac{\int_0^L \varphi(\zeta) f_n'(\zeta) d\zeta}{\int_0^L \varphi(\zeta) f_n(\zeta) d\zeta} \\ &= -\frac{\int_0^L \zeta f_n'(\zeta) d\zeta}{\int_0^L \zeta f_n(\zeta) d\zeta} \end{aligned} \tag{57}$$

A direct calculation gives that

$$\int_0^L \zeta f_n(\zeta) d\zeta = F_n \frac{L}{2} \qquad \text{and} \qquad \int_0^L \zeta f_n'(\zeta) d\zeta = -F_n \tag{58}$$

where $f_n(\zeta)$ as in (46). Finally,

$$\kappa = \frac{2}{L} \tag{59}$$

A more realistic model will assume that the deflection builds gradually but the rate of deflection build-up is reduced along the patch. This effect can be modeled by choosing $\varphi(\zeta) = \zeta^{\frac{1}{2}}$. Using such a φ and repeating the previous steps, one computes that

$$\kappa = \frac{7}{6}\frac{1}{L} \approx 1.1667 \frac{1}{L} \tag{60}$$

A more accurate estimate of κ can be computed assuming that the contact patch is divided into two separate regions, the adhesive region where friction gradually builds up, and the sliding region where the friction force has reached its maximum [24]. The adhesive region can be modeled by linear bristle deflection. In the sliding region the deflection of the bristles has reached a maximum. Therefore, we can choose the deflection function as $\varphi(\zeta) = b\,\mathrm{sat}(\zeta/b)$, where $0 < b < 1$ is a parameter that determines the transition between the sliding and adhesive regions of the contact patch. Using this expression for φ and tracing

the same steps as before, one obtains the following value of κ as a function of the parameter b

$$\kappa = \frac{2b(3-2b)}{L\,(b^3-2b^2+2)} \tag{61}$$

This expression is shown in Fig. 7(a). A comparison of several candidates for

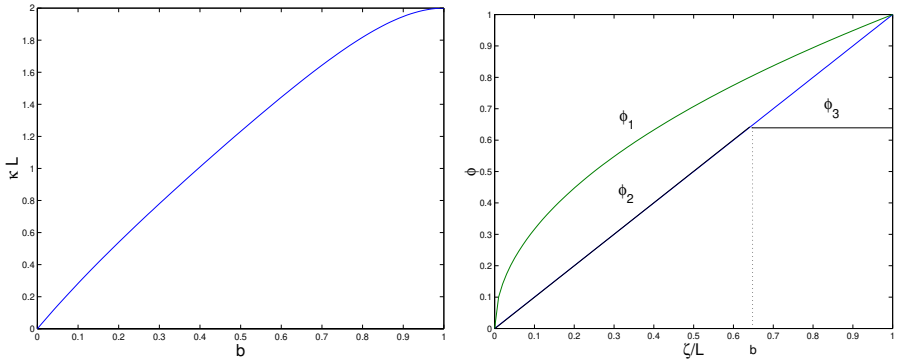

(a) (b)

Figure 7: (a): Variation of κL with b. Realistically, b varies between $0.3 \le b \le 0.9$. (b): Comparison of bristle deflection distribution function $\varphi(\zeta)$ along the patch for $\varphi_1 = \zeta^{\frac{1}{2}}$, $\varphi_2(\zeta) = \zeta$, $\varphi_3(\zeta) = b\,\mathrm{sat}(\zeta/b)$.

the bristle deflection function φ are shown in Fig. 7(b). Several other choices of the bristle deflection function $\varphi(\zeta)$ and the normal load distribution function $f_n(\zeta)$ can be used, yielding similar results. For most cases it is reasonable to chose κ in (53) to be a constant, somewhere in the range $1/L \le \kappa \le 2/L$.

Exponentially Decreasing Distribution

Assuming (42) along with $z(0,t) = 0$ one obtains

$$\begin{aligned}\kappa(t) &= \frac{1}{F_n\,\bar{z}}\Big[z(\zeta,t)e^{-\lambda(\zeta/L)}f_{n0}\Big]_0^L + \frac{1}{F_n\bar{z}}\int_0^L z(\zeta,t)\frac{\lambda}{L}e^{-\lambda(\zeta/L)}f_{n0}\,d\zeta \\ &= \frac{1}{F_n\bar{z}}z(L,t)e^{-\lambda}f_{n0} + \frac{\lambda}{L}\end{aligned} \tag{62}$$

Next, recall that we require $\lambda \ge 0$. For large values of λ it is possible to ignore the term containing $z(L,t)$ in the equation above, and approximate $\kappa(t)$ by a constant

$$\kappa = \frac{\lambda}{L}, \quad \text{with} \quad 0 \le \lambda \tag{63}$$

Uniform Normal Distribution

The case of the uniform normal distribution can be viewed as a special case of (42) with $\lambda = 0$. In this case $f_n(\zeta) = f_{n0} = F_n/L$ and we obtain the following expression

$$\kappa(t) = \frac{1}{F_n \bar{z}}\, z(L,t) f_{n0} = \frac{1}{L\bar{z}}\, z(L,t) \tag{64}$$

Deur [12] proposed that the boundary condition for the last element $z(L,t)$ be approximated by a linear expression of the average deflection $\bar{z}$,

$$z(L,t) \approx \kappa_0(t)\bar{z} \tag{65}$$

resulting in the relation,

$$\kappa(t) = \frac{\kappa_0(t)}{L} \tag{66}$$

The function $\kappa_0(t)$ in (65) is chosen in [12] so that the steady state solutions of the total friction force for the average/lumped model in (53)-(54), and the one of the distributed model (40) are the same. This approximation results in the following expression for κ_0

$$\kappa_0 = \kappa_0(Z) = \frac{1 - e^{-L/Z}}{1 - \frac{Z}{L}(1 - e^{-L/Z})} \tag{67}$$

In [12] it is also shown that, such a κ_0 belongs to the range $1 \leq \kappa_0(t) \leq 2$ for all $t \geq 0$. Often, a constant value for $\kappa_0 \in [1,2]$ can be chosen, without significantly changing the steady states of the distributed and lumped models. This can be verified from Fig. 8. Interestingly, this range of κ_0 is in agreement with the results of a parabolic normal load distribution; see Fig. 7(a).

Next, we present plots of the steady-state friction force as a function of the slip coefficient for the distributed model with uniform (Fig. 8(a)) and non-uniform normal load distribution (Fig. 8(b)), along with the steady-state plots of both average models.The parameters used for both models are shown in Table 2. All steady-state plots were made for constant vehicle velocity $v = 20\,\mathrm{m/sec}$ and patch length $L = 0.2\,\mathrm{m}$. For comparison, a fit with Pacejka's "Magic Formula" in (4) is also shown. The constants for Pacejka's formula were chosen as: $c_1 = 1, c_2 = 2, c_3 = 0.1, c_4 = 1$.

Table 2: Parameters used for Fig. 8.

Parameter	**Uniform Load**	**Non-uniform Load**
σ_0	395.86 m^{-1}	548.75 m^{-1}
σ_2	0.0012 sec/m	0.0022 sec/m
μ_c	0.93	0.93
μ_s	1.127	1.292
v_s	4.553 m/sec	3.7245 m/sec

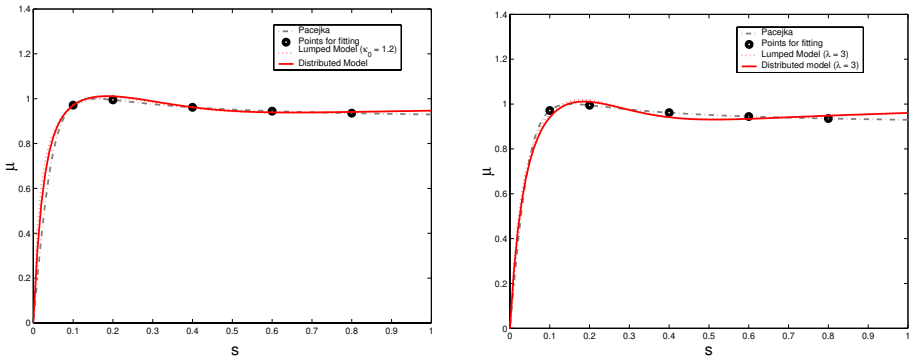

(a) (b)

Figure 8: Steady-state plots assuming: (a) uniform normal load distribution using the approximation from [12] with $\kappa_0 = 1.2$, and (b) the non-uniform normal load distribution given in (42) with $\lambda = 3$.

6 EXPERIMENTAL RESULTS

In this section we briefly present the measurements collected during three brakings of a specially equipped test vehicle. The measurements for the three brakings were taken under the same vehicle operational and road conditions. We have used this data to identify the parameters of the average/lumped LuGre tire friction model. We then used these parameters to validate the dynamic friction model by comparing the time histories of the friction force predicted by our model with the friction force measured during the experiments.

6.1 Testbed Car Description

The friction data were collected using the "BASIL" car which is a laboratory vehicle based on a Renault Mègane 110 Kw. The car is equipped with several sensors to study the behaviour of the vehicle during braking and traction phases. These sensors are (see Fig. 9):

- an optical cross-correlation sensor that measures the transverse and longitudinal vehicle velocities
- a basic inertial measurement unit with a piezoelectric vibrating gyroscope that measures the yaw rate; a separate sensor measures the roll velocity
- a magnetic compass that provides directional information
- two acceleration sensors that measure the longitudinal and lateral accelerations

- an ABS-system used to derive – via suitable signal processing – the wheels' velocities; the ABS system was not enabled during the experiments, it was used only as a wheel velocity sensor
- a differential GPS (DGPS) system used to locate the vehicle and compute its trajectory with great accuracy (less than one centimeter); this allows repeated experiments at the same road location
- other specific-purpose sensors (not described herein) used to measure the throttle angle (which reflects the command acceleration) and collector pressure (which reflects the braking command)

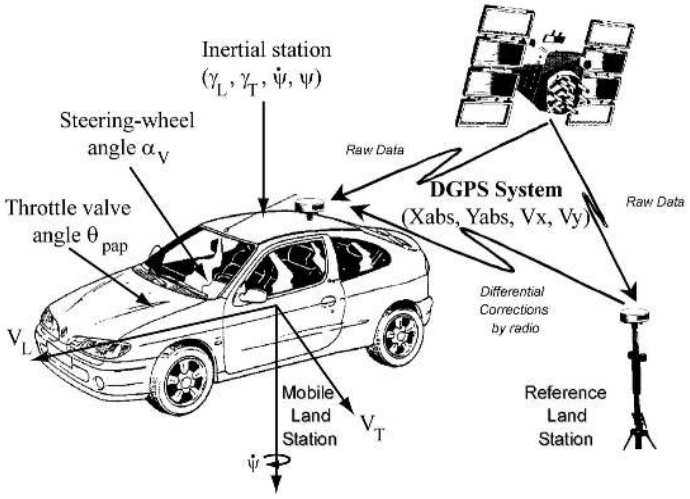

Figure 9: Sensors and measurement parameters.

For these experiments, a Wheel Force Transducer (WFT) was installed at center of the rim of the front right wheel (FRW) to measure the dynamic forces and moments acting between the road and the vehicle at the wheel center. Its inertial effects are small and hence they were neglected. This sensor gives the complete wrench in real time, namely the forces F_{xc}, F_{yc}, F_{zc} and the moment M_z. These are shown in Fig. 10. Although the WFT does not measure directly the friction forces and moments on the tire itself, it is assumed that the rim and tire dynamics can be neglected so that the forces and moments expressed at the contact patch (according to ISO 8855 specifications) can be calculated from the forces and moments at the wheel center via a simple coordinate transformation; see right drawing of Fig. 10. Such additional rim/tire dynamics can be added to the overall model, if desired. Since our main objective is to show the ability of the proposed friction model to capture the overall complex behaviour of the friction force and moment characteristics acting on the vehicle, it was not

deemed necessary to incorporate such higher order dynamics. Although more accurate, such an approach would unnecessarily dilute from the main results of this paper.

A schematic of the completely equipped "BASIL" vehicle, along with the corresponding measurement parameters is given in Fig. 9.

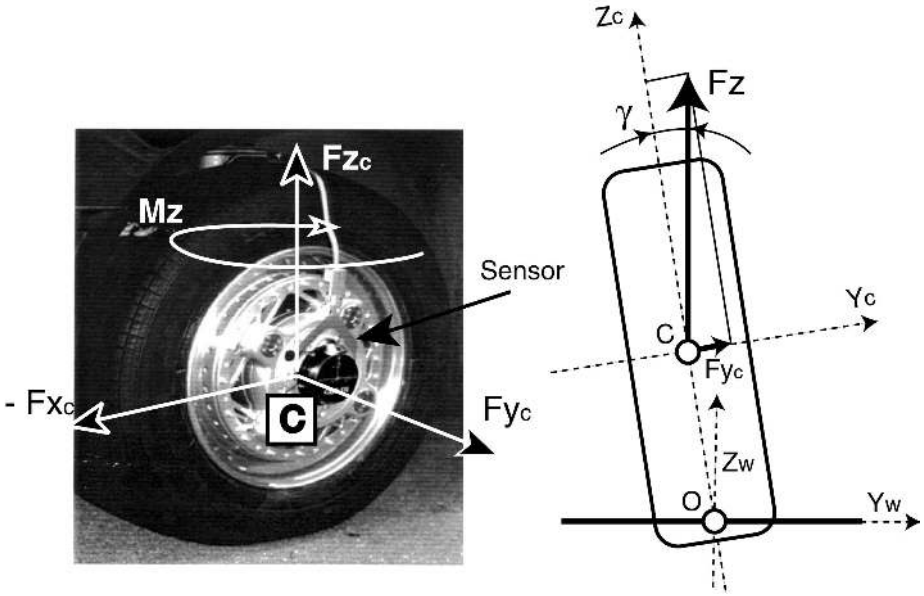

Figure 10: View of the equipped wheel with the Wheel Force Transducer (WFT); variables measured and axis systems used are according to ISO 8855 specifications. Rim and wheel dynamics are neglected so that the FWT forces are related to the actual forces at the contact patch via a simple coordinate transformation.

Experimental procedure

For safety reasons, trials were carried out on a straight, undeformed, flat and dry road. Before the braking phase, the following conditions where met:

- zero vertical load transferred
- slip velocity closed to zero
- steering wheel angle closed to zero
- F_x approximately constant and as small as possible

Most of these conditions may be reached (or approached) by removing the traction torque in the front wheels. For this, the driver releases the clutch for approximately two seconds, until the vehicle's speed decreases to a pre-specified value. Then, the test driver starts the braking phase and brakes strongly until

the grip limit of the front wheels is reached. Finally, he releases the brake pedal and the front wheels reach again normal grip conditions (small value of slip velocity). Then, the driver accelerates again to repeat the same sequence several times. Three such braking phases were performed and the results were stored in a file for subsequent analysis.

6.2 Collected Data

The collected data obtained from the experiments are shown in Figs. 11 and 12. Figure 11 shows a snapshot of the measurements of the braking pressure, the longitudinal speed of the vehicle and the front right wheel (FRW) velocity, for the three braking phases. Figure 12 shows the calculated forces F_{xw}, F_{yw}, F_{zw} at the contact patch, the calculated camber angle γ and the lateral acceleration G_t, for the test conditions specified above. The forces F_{xw}, F_{yw}, F_{zw} are derived from the projection of the measured forces F_{xw}, F_{yw}, F_{zw} in the $C-$frame onto the $W-$frame and they account for the camber and toe angle deviations (see Fig. 10).

The values of F_{yw} and G_t clearly show the low lateral excitation of the vehicle during braking. The peaks exhibited by these profiles are probably due to the geometrical characteristics of the suspension system that result in nonzero wheel camber angles and, in particular, to the toe angle compliance.

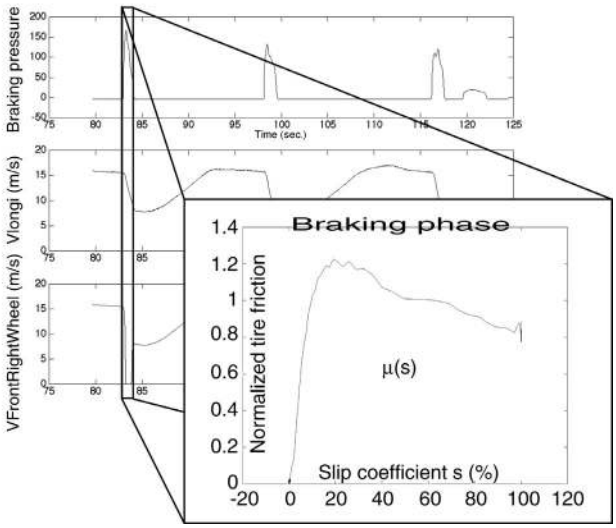

Figure 11: Braking experiments: measurements of the braking pressure, the longitudinal speed of the vehicle and the FRW velocity.

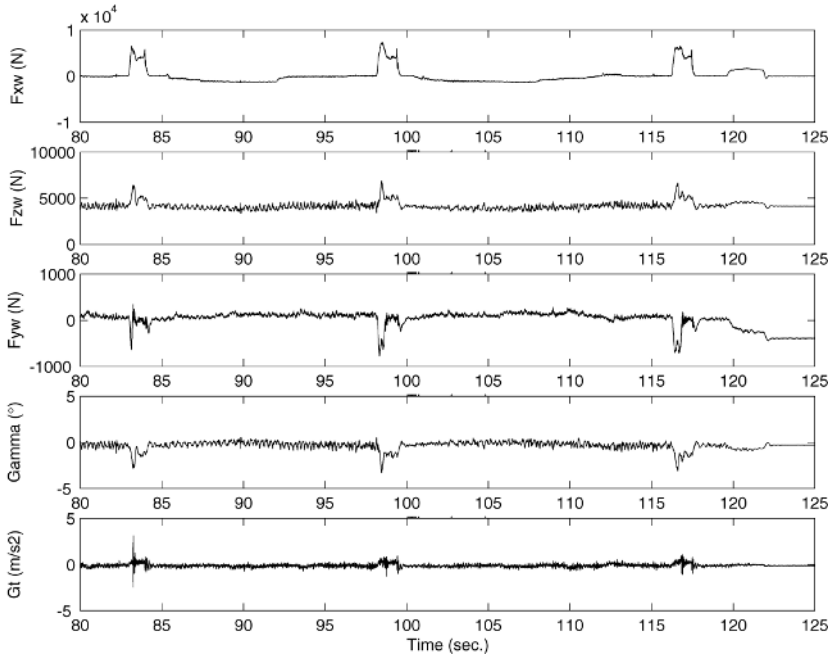

Figure 12: Braking experiments: time-profiles of the forces F_{xw}, F_{yw}, F_{zw}, the camber angle γ and the lateral acceleration G_t.

6.3 Parameter Identification

The experimental data consists of measurements of the longitudinal slip s, friction coefficient μ, and linear velocity v. We also know the sampling frequency of the measurements which allows us to re-construct the complete time vector history. The data used consists of three distinct brakings, shown in Fig. 12. Braking #1 consists of all data collected between 80 and 83.5 sec, Braking #2 consists of all data collected between 97 and 100 sec, and Braking #3 consists of the data collected approximately between 115 and 118 sec; see also the top plot of Fig. 12. First, we compared the (μ, s, v) steady-state solution of the distributed dynamical LuGre model at the mean velocity of one of the experiments (Braking #2) with the friction coefficient μ given by the experiments. We then used the $s-\mu$ plot of Braking #2 to identify the parameters for the steady state solution. We plotted the corresponding μ vs. slip curves and determined the parameters of the model ($\sigma_0, \sigma_2, \mu_s, \mu_c$ and v_s). By comparing the time histories of the friction force given by our model, with the ones given by the experiments we can determine the rest of the parameters (e.g., σ_1).

In order to identify the model parameters the `lsqnonlin` command of MATLAB was used by fitting the 3-D (μ,s,v) steady-state solution of the distributed model to the data of Braking #2. The command `lsqnonlin` solves an associated nonlinear least squares problem. The previous analysis was done for uniform

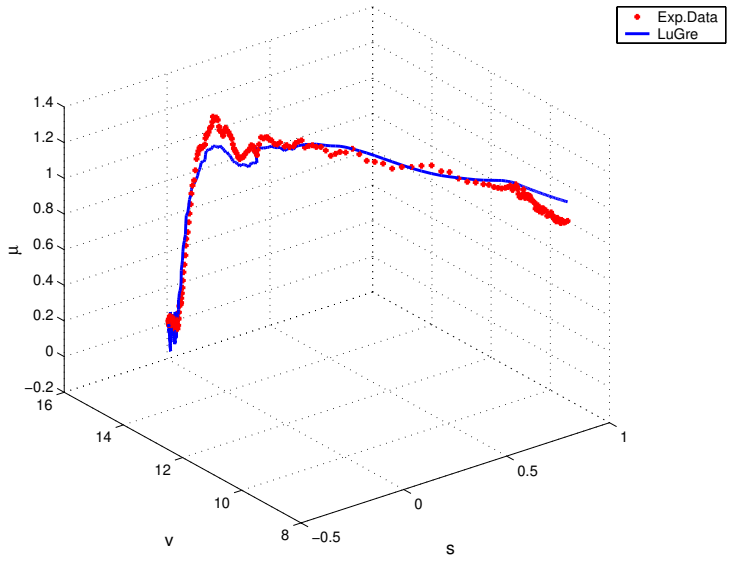

Figure 13: Three-dimensional plots of the corresponding (μ,s,v) curves for the collected data and the estimated predicted steady-state LuGre average lumped model, with $\alpha = 2$.

normal load distribution with $\kappa_0 = 1$ and 2 (case (i)), and with varying κ_0 (case (ii)). The case with exponential normal distribution (42) gives the same results as the ones in Fig. 14 and hence it is omitted. In all cases the patch length was chosen as $L = 0.2\,\mathrm{m}$. The results of the identification algorithm are shown in Table 3.

Table 3: Data used for the plots in Figs 14-15.

Parameter	**Value**
σ_0	178 m^{-1}
σ_1	1 m^{-1}
σ_2	0 sec /m
μ_c	0.8
μ_s	1.5
v_s	5.5 m/ sec

The comparison between the experimental results and the simulation results using the LuGre dynamic friction model for the three cases are shown in Figs. 14-15.

These figures indicate that our proposed model captures very well both steady-state and transient friction force characteristics.

7 CONCLUSIONS

In this paper we have revisited the problem of characterizing the friction at the tire/surface interface for wheeled vehicles. We have reviewed the major models used in the literature, namely, static, dynamic, lumped and distributed models. We have shown that static friction models are inadequate for describing the transient nature of friction build-up. Dynamic friction models are necessary to capture such transients during abrupt braking and acceleration phases. We propose a new dynamic friction model that accurately captures friction transients, as well as any velocity-dependent characteristics and tire/road properties. The model is developed by extending the well-known LuGre point friction model to the case of a contact patch at the tire/surface interface. Experimental results suggest that the proposed model, although simple, is accurate for analyzing tire friction. It is expected that this model will be useful both for simulation purposes, as well as for control design of ABS and TCS systems. Finally, it should be pointed out that although only the friction force along the longitudinal direction is addressed in this paper, the friction force for lateral/cornering or combined longitudinal/lateral motion can also be modeled using the ideas of this paper.

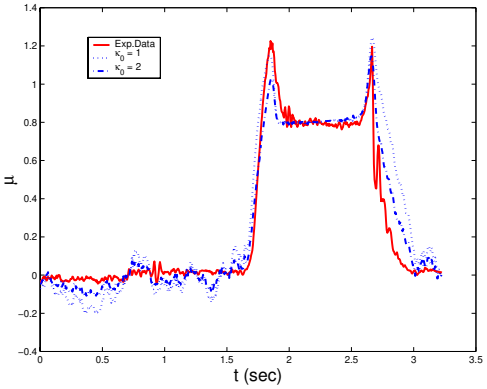

(a) Braking #1

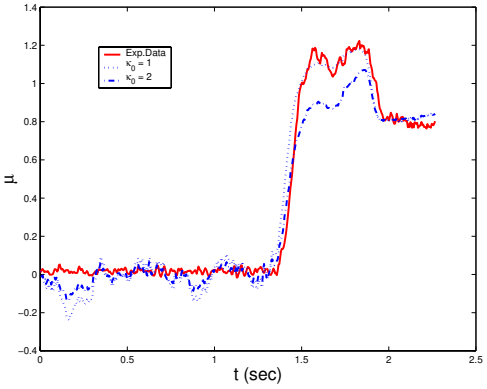

(b) Braking #2

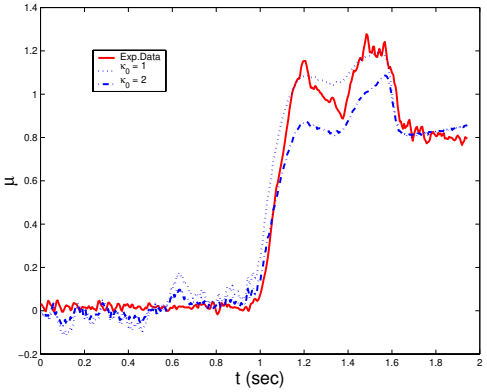

(c) Braking #3

Figure 14: Experimental and simulation results. Case (i): constant $\kappa_0 = 1, 2$.

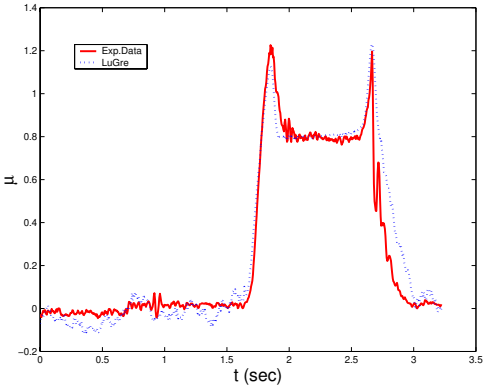

(a) Braking #1

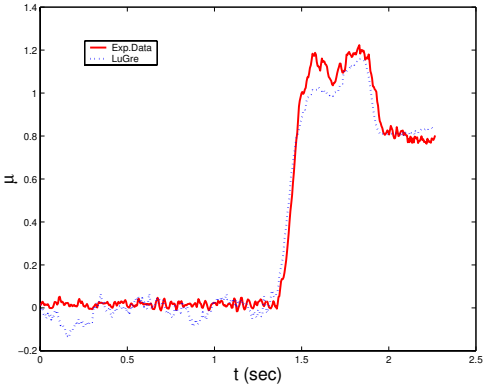

(b) Braking #2

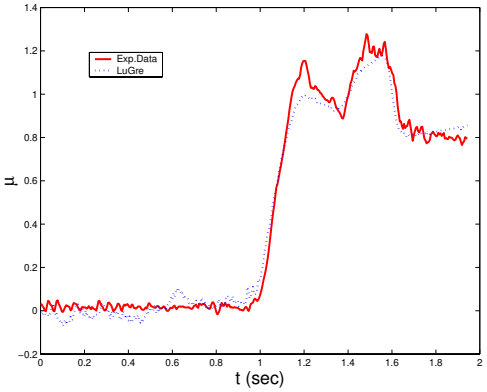

(c) Braking #3

Figure 15: Experimental and simulation results. Case (ii): varying κ_0.

ACKNOWLEDGEMENTS

The first two authors would like to acknowledge support from CNRS and NSF(award No. INT-9726621/INT-9996096), for allowing frequent visits between the School of Aerospace Engineering at the Georgia Institute of Technology and the Laboratory of Automatic Control at Grenoble, France. These visits led to the development of the dynamic friction model presented in this paper. The first author would like to thank M. Sorine and P.A. Bliman for interesting discussions on distributed friction models, and to X. Claeys for his remarks on the first version of the model. The second author also gratefully acknowledges partial support from the US Army Research Office under contract No. DAAD19-00-1-0473.

REFERENCES

1. Barahanov, N., and Ortega, R., "Necessary and Sufficient Conditions for Passivity of the LuGre Friction Model," *IEEE Transactions on Automatic Control*, Vol. 45, No. 4, pp. 830–832, 2000.
2. Bernard, J., and Clover, C. L., "Tire Modeling for Low-Speed and High-Speed Calculations," Society of Automotive Engineers, Paper 950311, 1995.
3. Bakker, E., Nyborg, L. and H. Pacejka, H., "Tyre Modelling for Use in Vehicle Dynamic Studies," Society of Automotive Engineers, Paper 870421, 1987.
4. Bliman, P.A., Bonald, T. and Sorine, M., "Hysteresis Operators and Tire Friction Models: Application to Vehicle Dynamic Simulations," *Proc. of ICIAM'95*, Hamburg, Germany, 3-7 July, 1995.
5. Burckhardt, M., "ABS und ASR, Sicherheitsrelevantes, Radschlupf-Regel System," *Lecture Scriptum*, University of Braunschweig, Germany, 1987.
6. Burckhardt, M., *Fahrwerktechnik: Radschlupfregelsysteme*, Vogel-Verlag, Germany, 1993.
7. Canudas de Wit, C., Olsson, H., Åström, K.J., and Lischinsky, P., "A New Model for Control of Systems with Friction," *IEEE Transactions on Automatic Control*, Vol. 40, No. 3, pp. 419–425, 1995.
8. Canudas de Wit, C., Horowitz, R. and Tsiotras, P., "Model-Based Observers for Tire/Road Contact Friction Prediction," In *New Directions in Nonlinear Observer Design*, Nijmeijer, H. and T.I Fossen (Eds), Springer Verlag, Lectures Notes in Control and Information Science, May 1999.
9. Canudas de Wit, C. and Tsiotras, P., "Dynamic Tire Friction Models for Vehicle Traction Control," In *Proceedings of the IEEE Conference on Decision and Control*, Phoenix, AZ, pp. 3746–3751, 1999.
10. Clover, C.L., and Bernard, J.E., "Longitudinal Tire Dynamics," *Vehicle System Dynamics*, Vol. 29, pp. 231–259, 1998.
11. Dahl, P.R., "Solid Friction Damping of Mechanical Vibrations," *AIAA Journal*, Vol. 14, No. 12, pp. 1675–1682, 1976.
12. Deur, J., "Modeling and Analysis of Longutudinal Tire Dynamics Based on the LuGre Friction Model," In *Proceedings of the IFAC Conference on Advances in Automotive Control*, Kalsruhe, Germany, pp. 101–106 ,2001.
13. Faria, L.O., Oden, J.T., Yavari, B.T., Tworzydlo, W.W., Bass, J.M., and Becker, E.B., "Tire Modeling by Finite Elements," *Tire Science and Technology*, Vol. 20, No. 1, pp. 33–56, 1992.
14. Gim, G. and Nikravesh, P.E., "A Unified Semi-Empirical Tire Model with Higher Accuracy and Less Parameters," *SAE International Congress and Exposition*, Detroit, MI, 1999.
15. Harned, J., Johnston, L. and Scharpf, G., "Measurement of Tire Brake Force Characteristics as Related to Wheel Slip (Antilock) Control System Design," *SAE Transactions*, Vol. 78, Paper 690214, pp. 909–925, 1969.

16. Kiencke, U. and Daiss, A., "Estimation of Tyre Friction for Enhaced ABS-Systems," In *Proceedings of the AVEG'94*, 1994.
17. Liu, Y. and Sun, J., "Target Slip Tracking Using Gain-Scheduling for Antilock Braking Systems," In *Proceedings of the American Control Conference*, pp. 1178–1182, Seattle, WA, 1995.
18. Maurice, J.P., Berzeri, M., and Pacejka, H.B., "Pragmatic Tyre Model for Short Wavelength Side Slip Variations," In *Vehicle System Dynamics*, Vol. 31, pp. 65–94, 1999.
19. Moore, D.F., *The Friction of Pneumatic Tyres*, Elsevier Scientific Publishing Co., New York, 1975.
20. Pasterkamp, W.R. and Pacejka, H.B., "The Tire as a Sensor to Estimate Friction," *Vehicle Systems Dynamics*, Vol. 29, pp. 409–422, 1997.
21. Pacejka, H.B. and Sharp, R.S., "Shear Force Developments by Pneumatic Tires in Steady-State Conditions: A Review of Modeling Aspects," *Vehicle Systems Dynamics*, Vol. 20, pp. 121–176, 1991.
22. Ramberg W., and Osgood W.R., "Description of Stress-Strain Curves by Three Parameters," *Technical Note 902*, National Advisory Committee for Aeronautics, Washington, DC, 1943.
23. Sargin, M., "Stress-Strain Relationship for Concrete and the Analysis of Structural Concrete Sections," *SM Study 4*, Solid Mechanics Division, University of Waterloo, Canada, 1971.
24. Wong J.Y., *Theory of Ground Vehicles*, John Wiley & Sons, Inc., New York, 1993.
25. van Zanten, A., Ruf, W.D., and Lutz, A., "Measurement and Simulation of Transient Tire Forces," In *International Congress and Exposition*, Detroit, MI, SAE Technical Paper Series, Paper 890640, 1989.

APPENDIX A: DISTRIBUTED MODEL DERIVATION

Let $z(\zeta, t)$ denote the friction state (deflection) of the bristle/patch element located at the point ζ along the patch at a certain time t and consider the total deflection of this element between two time instances t and $t+dt$. Since the time interval dt the element has moved to the location $\zeta + d\zeta$, and using (24)-(25), we have that (see also Fig. 16)

$$z(\zeta + d\zeta, t + dt) - z(\zeta, t) = (v_r - \frac{\sigma_0 |v_r|}{g(v_r)} z(\zeta, t))\, dt$$

The total deflection is given by $dz = z(\zeta + d\zeta, t + dt) - z(\zeta, t)$. Since

$$dz = \frac{\partial z}{\partial \zeta} d\zeta + \frac{\partial z}{\partial t} dt$$

substituting in the previous equation, one obtains

$$\frac{\partial z}{\partial t}(\zeta, t) + \frac{\partial z}{\partial \zeta}(\zeta, t) \frac{d\zeta}{dt} = v_r - \frac{\sigma_0 |v_r|}{g(v_r)} z(\zeta, t)$$

Using the fact that $d\zeta/dt = |\omega r|$ we have the following partial differential equation for the internal friction state along the patch

$$\frac{\partial z}{\partial t} + \frac{\partial z}{\partial \zeta} |\omega r| = v_r - \frac{\sigma_0 |v_r|}{g(v_r)} z$$

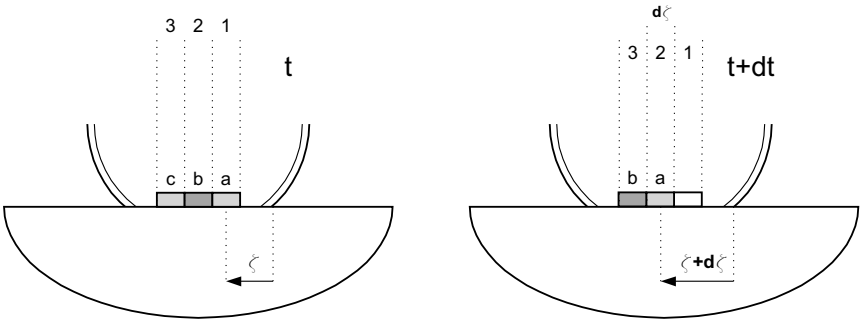

Figure 16: Derivation of distributed friction model along the contact patch.

The friction force generated at the patch can be computed from

$$F(t) = \int_0^L dF(\zeta, t)$$

where $dF(\zeta, t)$ is the friction force developed in the element of length $d\zeta$, located at position ζ of the patch, at time t and given by the point LuGre model as

$$dF(\zeta, t) = \left(\sigma_0 z(\zeta, t) + \sigma_1 \frac{\partial z}{\partial t}(\zeta, t) + \sigma_2 v_r \right) f_n(\zeta)$$

where $f_n(\zeta)$ is the normal force density function (normal force per unit length) along the patch. The total friction force at the patch, can thus be computed as follows

$$F(t) = \int_0^L (\sigma_0 z(\zeta, t) + \sigma_1 \frac{\partial z}{\partial t}(\zeta, t) + \sigma_2 v_r) f_n(\zeta)\, d\zeta$$

APPENDIX B: DECREASING NORMAL FORCE DISTRIBUTION EQUATION

In this appendix we give the details for deriving equation (43). Starting from (38) and assuming (42) we get for the first term in (38)

$$\begin{aligned}
\int_0^L \sigma_0 z_{ss}(\zeta) f_n(\zeta)\, d\zeta &= \sigma_0 \int_0^L c_2 (1 - e^{c_1 \zeta}) f_{n0} e^{-\lambda(\frac{\zeta}{L})} d\zeta \\
&= \sigma_0 c_2 f_{n0} \int_0^L (1 - e^{c_1 \zeta}) e^{-\frac{\lambda}{L}\zeta} d\zeta \\
&= \sigma_0 c_2 f_{n0} \Big[-\frac{L}{\lambda} e^{-\frac{\lambda}{L}\zeta} - \frac{L}{c_1 L - \lambda} e^{(c_1 - \frac{\lambda}{L})\zeta} \Big]_0^L \\
&= \sigma_0 c_2 f_{n0} \left(-\frac{L}{\lambda} e^{-\lambda} - \frac{L}{c_1 L - \lambda} e^{(c_1 L - \lambda)} + \frac{L}{\lambda} + \frac{L}{c_1 L - \lambda} \right)
\end{aligned}$$

$$
\begin{aligned}
&= \sigma_0 c_2 f_{n0} \frac{L}{\lambda}\left(1 - e^{-\lambda} - \frac{\lambda}{c_1 L - \lambda} e^{(c_1 L - \lambda)} + \frac{\lambda}{c_1 L - \lambda}\right) \\
&= \sigma_0 c_2 f_{n0} \frac{L}{\lambda}\left(1 - e^{-\lambda} + \frac{\lambda}{c_1 L - \lambda}(1 - e^{(c_1 L - \lambda)})\right)
\end{aligned}
$$

Similarly, for the second term in (38) we have that

$$
\begin{aligned}
\int_0^L \sigma_2 v_r f_n(\zeta) d\zeta &= \sigma_2 v_r \int_0^L f_n(\zeta) d\zeta = \sigma_2 v_r \int_0^L e^{-\lambda(\frac{\zeta}{L})} f_{n0} d\zeta \\
&= -\sigma_2 v_r f_{n0}\Big[\frac{L}{\lambda} e^{-\lambda(\frac{\zeta}{L})}\Big]_0^L = \sigma_2 v_r f_{n0}\Big[\frac{L}{\lambda} - \frac{L}{\lambda} e^{-\lambda}\Big] \\
&= \sigma_2 v_r \frac{f_{n0} L}{\lambda}(1 - e^{-\lambda})
\end{aligned}
$$

Finally,

$$
F_{ss} = \sigma_0 c_2 k_1\Big(1 - e^{-\lambda} + k_2 e^{(\lambda + c_1 L)} + k_2\Big) + \sigma_2 v_r k_1 (1 - e^{-\lambda})
$$

where the constants k_1 and k_2 are given by

$$
k_1 = \frac{f_{n0} L}{\lambda} \qquad \text{and} \qquad k_2 = \frac{\lambda}{c_1 L - \lambda}
$$